Appl. Phys. B 50, 441–454 (1990)

Applied Physics B Photophysics and Laser Chemistry

Planar Laser-Fluorescence Imaging of Combustion Gases

Ronald K. Hanson, Jerry M. Seitzman, and Phillip H. Paul

High Temperature Gasdynamics Laboratory, Department of Mechanical Engineering, Stanford University, Stanford, CA 94305, USA

Received 22 December 1989/Accepted 20 March 1990

Abstract. An overview is provided of the planar laser-induced fluorescence (PLIF) method, which currently allows simultaneous combustion measurements at more than 10^5 flowfield points. Important advantages of the method include its relatively high signal strength, ease of interpretation, and applicability for determining several flowfield variables (including concentration, temperature, velocity, pressure and density). Example results are shown for a turbulent non-premixed flame, a spray flame, a rod-stabilized premixed flame, and a diffusion flame from a fuel jet in cross-flow.

PACS: 07.65, 33, 42.80

Combustion measurements techniques based on planar imaging of scattered laser light provide a powerful complement to single-point laser diagnostics and conventional flow visualization methods. Fluorescence-based imaging is particularly attractive owing to the strength of the process, relative to its primary competitors, Rayleigh and Raman scattering, and to its potential for monitoring several flowfield parameters. For example, planar laser-induced fluorescence (PLIF) imaging has already been suggested or demonstrated for instantaneous, i.e. single laser shot, non-invasive monitoring of species concentration, temperature, velocity, pressure and density; and images with simultaneous measurements at up to 10^6 flowfield points are feasible with current solid-state cameras. The aim of this paper is to provide a concise overview of the PLIF method and to illustrate its status and potential through example results obtained in our laboratory.

The general arrangement for PLIF imaging is shown in Fig. 1. A laser source, usually pulsed and tunable in wavelength, is used to form a thin sheet of light which traverses the flowfield under study. If the laser photon energy is resonant with an optically allowed quantum transition of a species present in the flow, a fraction of the incident photons will be absorbed at each point within the illumination plane. A fraction of these absorbed photons may subsequently be re-emitted with a modified spectral distribution; these photons, known as "fluorescence", may be viewed as a form of molecular scattering and constitute the signal of interest in PLIF imaging. Although the fluorescence is emitted into 4π steradians, a useful fraction of the light may be collected and imaged onto a sensitive, usually image-intensified, solid-state camera. The fluorescence intensity distribution in the

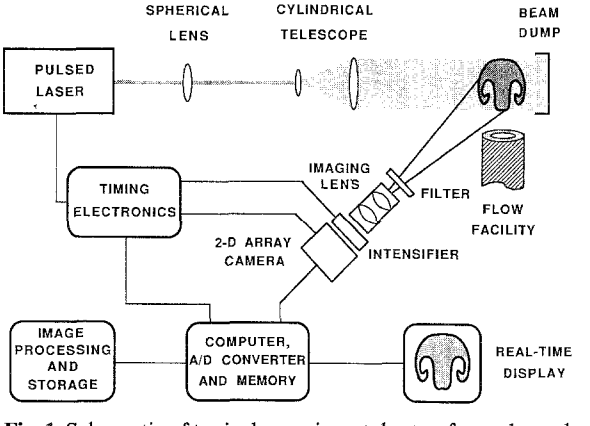

Fig. 1. Schematic of typical experimental setup for a planar laser-induced fluorescence (PLIF) experiment

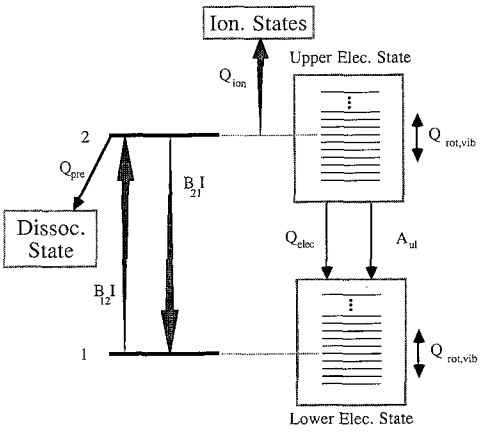

Fig. 2. Critical energy transfer processes in laser-induced fluorescence (LIF). Included are rate coefficients for spontaneous emission from the upper to lower electronic manifolds (A_{ul}), stimulated absorption ($B_{12}I$) and emission ($B_{21}I$) between single energy levels in the two manifolds, photoionization (Q_{ion}), and collisional energy transfer, rotational and vibrational ($Q_{rot,vib}$), electronic (Q_{elec}) and predissociation (Q_{pre}). In this diagram, energy levels are depicted by horizontal lines and boxes represent energy manifolds, for example an electronic state with many rotational and vibrational energy levels. Large arrows indicate laser-stimulated processes

illumination plane recorded by the camera essentially provides an image of the product of absorber number density in a particular quantum state and the local fluorescence yield, i.e. the fraction of absorbed light converted to fluorescence. By various strategies, this signal can be related to other flowfield properties of interest. The temporal resolution of the measurement in atmospheric-pressure (and higher) combustion is effectively controlled by the laser source, with 5–20 ns pulse lengths being typical. The greatest achievable spatial resolution of the image is set by the sensor array, which may contain from ten thousand to more than one million picture elements (pixels).

Fluorescence imaging may be viewed as a modern form of flow visualization. In common with methods such as schlieren and shadowgraphy, PLIF is extremely useful for qualitative characterization of complex flowfields, but it has the important added capabilities of species specificity and of providing spatially resolved information in a plane rather than integrated over a line-of-sight. The former characteristic is critical for studies of reacting flows, while the latter quality is important for resolving three-dimensional flowfield structure. The fact that PLIF involves excitation of specific quantum states in individual species provides a means of sensing temperature through the relevant Boltzmann distribution. The use of fluorescence monitoring of Doppler-shifted molecular absorption has enabled direct imaging of 2-D gas velocities in non-reacting flows without the use of particulate seeding; the same approach should also be applicable in combustion flows. Other variations of PLIF allow imaging of pressure and density.

The history of fluorescence imaging is brief. Following pioneering work on planar imaging of Rayleigh-scattered laser light at Yale [1] in the late 1970s, linear and planar variations of laser-induced fluorescence imaging of species concentration were reported by three groups in 1982 [2–4]. Subsequent important extensions of PLIF include demonstration of species imaging in evaporating [5] and burning fuel sprays [6], temperature imaging in gases [7, 8], velocity imaging [9, 10], and combined velocity/pressure imaging [11]. An overview of early work on PLIF and other planar imaging methods, complete through 1986, was given previously [12]. Activity to develop and apply PLIF imaging is growing, and significant advances may be expected, owing both to the potential of PLIF diagnostics and to ongoing improvements in solid-state camera systems, tunable lasers and image processing equipment.

1. Basic Principles of Laser-Induced Fluorescence

Laser-induced fluorescence, LIF, is a well-established, sensitive technique for detecting population densities of atoms and molecules in specific quantum states. Although LIF was used initially in studies of spectroscopy and chemical analysis, it is now also recognized as a powerful combustion diagnostic with the potential for monitoring parameters such as species concentration, mixture mole fractions, density, temperature, velocity and pressure. The early development of LIF methods was driven by single-point measurements, but the underlying concepts carry over directly to multiple-point planar imaging. This section describes the basic physical processes involved in an LIF experiment and presents some simple models which are useful in relating fluorescence measurements to interesting combustion parameters.

Generally, fluorescence denotes the radiation emitted by a molecule or atom when it decays by spontaneous emission of a photon in an "allowed" transition from a higher to lower energy state. In a laser-induced fluorescence measurement, the upper state is populated by a laser source with an emission frequency tuned to a resonance between the excited state and a discrete lower state. Typically, the lower state is in the ground electronic level, as the other electronic levels may be negligibly populated at combustion temperatures.

After excitation, the laser-populated upper state may undergo a number of subsequent processes. Figure 2 depicts five important mechanisms in LIF of a

molecular species, molecules being more representative of combustion PLIF applications than atoms. Firstly, the molecule can be returned to its original quantum state by (laser-induced) stimulated emission. Secondly, absorption of an additional photon can excite still higher molecular states, including ionized levels. Thirdly, the internal energy of the system can be altered in inelastic collisions with other molecules, producing rotational and vibrational energy transfer, and also electronic energy transfer; the latter is often referred to as quenching. Fourthly, interactions between the separate atoms of the molecule, known as "internal" or "half" collisions, produce internal energy transfer and dissociation of the molecule. When the dissociation is produced by a change from a stable to a repulsive electronic arrangement in the molecule, it is called predissociation, as shown in Fig. 2. Finally, the originally populated state, and nearby upper states indirectly populated through collisions, fluoresce, producing the LIF signal.

The LIF signal can be related to specific properties (e.g., concentration and temperature) of the absorbing species through modeling of these state-to-state transfer processes. As the fluorescence is a function of the upper state's population, this requires solving the state-dependent population dynamics. While quantum-mechanical density-matrix descriptions of the interactions involved in LIF are available [13–14], most treatments of LIF [15, 16] are based on a semiclassical rate equation analysis developed by Piepmeir [17]. The rate equations are conceptually and mathematically more tractable than the quantum approach, but fail to include possible coherence effects. Generally in combustion measurements, the validity of the rate equation analysis holds for laser pulses which rise slowly compared to the characteristic collision time, 10–100 ps in atmospheric-pressure flames [18]. Even when this condition is not met, the multimode nature of typical excitation lasers can tend to mask coherence effects [19].

The formal rate equation governing the time-dependent population, $n_j(t)$ [cm^{-3}], of a specific energy level among a set of levels, i, is given by

$$dn_j(t)/dt = \sum_{i \neq j} n_i(t) R_{ij} - n_j(t) \sum_{i \neq j} R_{ji}, \tag{1}$$

where the first summation represents events which populate j while the second denotes loss processes. The total rate coefficient for all events transferring molecules from level i to j is R_{ij} [s^{-1}]. A number of distinct rate coefficients are included in this overall coefficient: the collisional transfer coefficient Q_{ij}, encompassing both intermolecular and internal collisions; the Einstein A coefficient A_{ij}, for spontaneous emission (i.e. fluorescence); and the coefficient for single-photon laser stimulated processes, $B_{ij}I_\nu$, where I_ν [$W\,cm^{-2}\,Hz^{-1}$] is the laser spectral intensity and B_{ij} is the Einstein B coefficient. In analyzing these rate equations, it is useful to recognize that spontaneous emission occurs only if level i is greater in energy than j (i.e., $A_{ij}=0$ for $E_j > E_i$), and that the laser stimulated rates are related by the principle of detailed balance, $g_i B_{ij} = g_j B_{ji}$ where g_i is the degeneracy of level i. In (1), we have assumed that the laser source has a characteristic spectral bandwidth which is broad compared to the bandwidth of the molecular transition, i.e., the laser spectral intensity is constant across the molecular absorption line. This broadband laser model is appropriate for most pulsed laser sources, since their spectral widths tend to be larger than widths of molecular transitions in PLIF flame measurements. More complicated, frequency dependent approaches [17, 20, 21], which allow for "hole-burning" of inhomogeneously broadened transitions, must be used for narrowband laser sources. Fortunately, the simpler broadband model reveals most of the fundamental concepts in LIF.

To illustrate the essential properties of LIF, it is common to simplify (1) to the case of a two-level molecular system, based on the two levels coupled by the laser radiation. For this two-level model, the rate equation for the upper energy level becomes

$$dn_2(t)/dt = n_1(t)[Q_{12} + B_{12}I_\nu] - n_2(t)[Q_{21} + B_{21}I_\nu + A_{21}]. \tag{2}$$

As suggested previously, the upper level typically has a negligible population prior to the laser pulse, so the initial condition, $n_2(t=0)=0$, is applied to (2). Additionally there is a conservation constraint on the total population, i.e., no chemical reactions occur during the measurement,

$$n_1(t) + n_2(t) = \text{constant} = n_1^0, \tag{2}$$

where n_1^0 is the initial population of n_1. The solution to the two-level system is given by

$$n_2(t) = n_1^0 [B_{12}I_\nu + Q_{12}]\tau[1 - e^{-t/\tau}], \tag{4}$$

where the time constant τ is $[B_{12}I_\nu + Q_{12} + (g_1/g_2)B_{12}I_\nu + Q_{21} + A_{21}]^{-1}$. For laser pulses long compared to τ, the system reaches steady state, and the steady-state fluorescence rate R_p [number of photons/cm^3/s] is

$$R_p = A_{21} n_0^{ss} = A_{21} n_1^0 [B_{12}I_\nu + Q_{12}]\tau. \tag{5}$$

The two laser-coupled energy levels are typically separated by a few electron-volts, thus collisional excitation (Q_{12}) can be omitted in most combustion environments. The steady-state fluorescence rate is

thus more conveniently written

$$R_p = n_1^0 B_{12} I_\nu \frac{A_{21}}{A_{21}+Q_{21}} \frac{1}{1+I_\nu/I_\nu^{sat}}, \quad (6)$$

where the saturation intensity I_ν^{sat} is defined as

$$I_\nu^{sat} = \frac{Q_{21}+A_{21}}{B_{12}(1+g_1/g_2)}. \quad (7)$$

Equation (6) can be further simplified for two limiting cases, corresponding to either low or high laser intensity. For low laser intensities ($I_\nu \ll I_\nu^{sat}$), (6) reduces to

$$R_p = n_1^0 B_{12} I_\nu \frac{A_{21}}{A_{21}+Q_{21}}. \quad (8)$$

This is the so-called linear fluorescence equation, as the fluorescence is linearly proportional to laser intensity. For high intensities ($I_\nu \gg I_\nu^{sat}$), the result approaches the "saturation limit"

$$R_p = n_1^0 \frac{A_{21}}{1+g_1/g_2}. \quad (9)$$

Typically, the linear fluorescence equation is used to model PLIF combustion measurements.

Equation (8) shows the fluorescence signal to be proportional to the unperturbed lower state population and to a factor $A_{21}/(Q_{21}+A_{21})$, known as the Stern-Vollmer factor or fluorescence yield. For this reason, LIF may be considered to be a measurement of the lower state population, modified by the fluorescence yield. Through the influence of the fluorescence yield, upper state collisional decay processes can be important in relating the LIF signal to the desired flowfield parameters whenever $Q_{21} \gg A_{21}$, as is usually the case near and above atmospheric pressure. As molecular collision rates are sensitive to pressure, temperature and composition, variations in Q_{21} may be difficult to predict in some reacting flows, thereby limiting quantitative applications of PLIF for species concentration imaging. In some cases, the upper state decay rate is dominated by other processes which are insensitive to molecular collisions. One example is an upper state which predissociates at a rate exceeding the molecular collision rate [22]. Alternatively, the upper state's decay rate can be controlled by laser-stimulated photoionization [23, 24], as illustrated in Fig. 2. Measurements of some parameters, such as temperature and velocity, can be made by taking combinations of fluorescence signals in a way that cancels the collisional dependence [11, 25].

The fluorescence rate is converted to a total fluorescence signal by temporal integration over the laser pulse duration and by inclusion of the collection efficiency of the detection optics. Assuming the fluorescence is emitted equally into 4π steradians (see below), the total number of photons N_p striking a photodetector from the collection volume V_c, the volume image onto the detector, is

$$N_p = \eta \frac{\Omega}{4\pi} f_1(T) \chi_m n V_c B_{12} E_\nu \frac{A_{21}}{A_{21}+Q_{21}}, \quad (10)$$

where η is transmission efficiency of the collection optics, Ω is the collection solid angle, $f_1(T)$ is the fractional population of the lower laser-coupled state, χ_m is the mole fraction of the absorbing species, n is the total gas number density and E_ν [J cm^{-2} Hz^{-1}] is the spectral fluence of the laser.

Although (10) was derived for a system in which only the two levels coupled by the laser undergo population transfer during the laser pulse, a real molecular system may behave in this way if the transfer rates between the two states are much faster than rates to nearby (e.g., rotational) states. Equation (10) also accurately models real molecular systems for a number of other conditions. Multilevel models are satisfied by (10) when the population transfer out of levels 1 and 2 is balanced by transfer in from surrounding states [26]. Equation (10) may also be valid when broadband detection of fluorescence, not only from the laser-excited state but also from all states collisionally coupled to it, is used. This is true if rotational transfer in the upper electronic state is fast, or if the lower level is weakly perturbed ($n_1 = n_1^0$), e.g., owing to fast repopulation of the lower rotational level through rotational transfer from nearby levels. In both these cases, the LIF signal is again given by (10), with A_{21} replaced by an effective fluorescence rate. This effective rate may have some collisional dependence if the fluorescing states have different A coefficients. Broadband detection also reduces polarization effects [27], such that the assumption of equal radiation into 4π steradians is sufficiently accurate.

Implicit in the above development was the assumption that the laser radiation has no perturbing effect on the parameters being measured. There are cases, however, where the laser does perturb local combustion parameters, such as the temperature, since the absorption of laser radiation acts as an energy input mechanism, or the chemical structure, through the photo-production of radicals. In LIF measurements of O atoms in flames, Miziolek and DeWilde [28] found that the LIF laser was significantly altering the O concentration during the measurement, through multiphoton dissociation of the fuel and oxidizer. Similar results have been reported by Goldsmith [29]. In some cases, laser-induced photodissociation may be usefully applied to measure the concentration of parent molecules. For example, the fragments of the

parent molecule may be produced in excited electronic states, which subsequently emit detectable fluorescence [30]. For situations in which the dissociated fragments are produced in ground or non-fluorescing states, a second LIF probe laser can be used to monitor the fragment distribution [31]. In either case, determination of the fragment concentration may be related to the original parent molecule's concentration if the photodissociation rate coefficient is known.

2. Equipment Considerations

As illustrated in Fig. 1, the hardware required to implement PLIF can be divided into three subsystems: the excitation, detection, and processing/computing systems. The excitation system consists of a laser illumination source and associated sheet forming optics. The detection system includes collection optics (e.g., lenses and spectral filters), a two-dimensional array detector (often image-intensified), and amplification, digitization and control electronics. The processing subsystem is an image analysis computer which may be used after the actual measurement, in a post-processing mode, or may be used for real-time image processing. Comments on excitation and detection systems follow below.

2.1. Excitation System

Many laser sources, with widely varying capabilities, are currently available; an excellent description of lasers for spectroscopic applications is given by Demtröder [14]. The most common laser system used in PLIF measurements are Nd:YAG-pumped, excimer-pumped, and flashlamp-pumped pulsed dye lasers; excimer and Raman-shifted excimer lasers; and less commonly, ion lasers and ion-pumped dye lasers. The following characteristics of laser sources are the most important for PLIF applications: center frequency, bandwidth (no light source is completely monochromatic), tunability, energy or intensity, temporal behavior, and beam quality (e.g., spatial uniformity and beam divergence).

As explained previously, LIF is a resonance process; production of reasonable signal levels requires that the laser frequency must closely overlap a resonant transition in the species of interest. In some cases, fixed-frequency lasers exhibit such overlaps, e.g., the Ar^+ ion laser with I_2, or the ArF excimer laser with O_2 and NO; generally, tunable dye lasers must be used. Additionally, frequency conversion techniques such as frequency-mixing in optical crystals, and Raman-shifting may be useful. Laser bandwidths are also an important consideration for improving the signal-to-noise ratio (SNR). A laser with a spectral distribution which is much wider than the spectral width of the transition(s) being excited exhibits less efficient radiative coupling and produces weaker LIF signals.

In most PLIF applications, pulsed lasers are the preferred illumination source, as their short pulse lengths along with typically short fluorescence lifetimes, less than 100 ns, provide the ability to freeze motion in the flowfield. Their high intensities can increase the SNR in flowfields with significant background luminosity, by permitting short detector integration times. The repetition rate of these lasers is generally 10 Hz to 500 Hz, which limits the achievable recording rate. Continuous wave (cw) lasers potentially allow recording rates limited only by detector framing rates. Typically, though, cw lasers have low intensities, so the integration time needed to obtain a reasonable SNR produces poor temporal resolution and degrades the spatial resolution through image-smearing. In some situations, where very high speed recording rates are desired, a possible compromise between pulsed and cw sources is a long-pulse laser. For the duration of a number of frames with high framing rate, fast-gating imaging detectors, the laser pulse (1–100 μs for a flashlamp-pumped dye laser) is effectively cw.

The laser beam may be formed into a sheet with various optical systems. The chosen optical system should produce a sheet of approximately uniform illumination. Although intensity non-uniformities can be corrected in the imaging processing system, the correction usually results in some degradation of spatial and signal resolution. Frequently, the sheet optics consist of two or three lenses. A long focal length spherical lens loosely focuses the beam, ensuring that the beam thickness varies little over the imaged region. Two cylindrical lenses spread the beam into a collimated sheet; one spreads the beam while the second collimates it. A single cylindrical lens can be used if the sheet spreading angle produces an insignificant change in intensity across the imaged portion of the flow.

In some situations, it is desirable to use a multipass arrangement to produce the illumination sheet, as this produces a sheet of higher intensity. Such an arrangement can be as simple as a single mirror, which reflects the sheet back on itself, or may consist of a pair of cylindrical mirrors. In the latter arrangement, a small sheet is focused midway between the two mirrors, and the mirrors are aligned so as to have the beam "walk" down and up the mirrors, refocusing on each pass [32].

2.2. Detection System

In general, the fluorescence from a portion of the illuminated plane is collected by an imaging lens at

right angles, passed through a spectral filter, and imaged directly onto a two-dimensional photodetector or onto the front face of an image intensifier, optically coupled to a two-dimensional array detector. The two-dimensional array is then scanned, the analog output voltage amplified, and the result digitized or recorded as an analog signal.

Simple lenses may be used to collect laser-induced fluorescence, though aberration-corrected lens systems provide improved spatial resolution when imaging, especially in low f-number applications. Commercial camera lenses are designed to be diffraction limited, that is effectively free of both monochromatic and chromatic aberrations, over a range of conjugate ratios, f-numbers and wavelengths. With such lenses, especially at low f-number, focussing errors, i.e. depth-of-field problems, usually limit the spatial resolution achieved [33].

In selecting a lens system, the major tradeoff is between spatial response and light-gathering ability. A typical compromise is to use a sufficiently small f-number to produce a lens resolution equal to the spatial resolution of the other camera system components, as this gives the maximum collection efficiency without seriously degrading the spatial response. Again for a more detailed discussion, see the paper by Paul et al. [33].

The collected fluorescence can either be imaged directly onto a two-dimensional photodetector or onto the photocathode of an image tube. We use the term image tube to describe imaging devices in which photons incident on a photocathode are converted to photoelectrons. The photoelectrons are accelerated away from the photocathode by an applied voltage, which can be quickly switched or gated. Finally, electrons are accelerated onto a phosphor coated surface, creating new photons and reproducing the original image. In special image tubes, known as image intensifiers, the photoelectrons undergo cascade amplification before striking the phosphor, thereby leading to an output image brighter than the original image. Typically, the electrons leaving the photocathode are accelerated by a few hundred volt potential towards a thin microchannel-plate, MCP [34]. The coated glass MCP material is similar to that of photomultiplier tube dynodes and contains many (usually millions) of small diameter ($\approx 10\,\mu m$) channels. The photoelectrons collide with the channel walls, producing secondary electrons and resulting in a cascade growth in the number of electrons. Intensifiers are available in single and multiple MCP configurations; the latter have higher electron gains than single MCP designs, but this is offset by the lower spatial resolution resulting from stacking the MCPs.

Image tubes serve three basic functions. They act as photon amplifiers, as fast (as short as 1 ns) gates or "shutters," and as wavelength converters. As amplifiers, they are useful in detecting fluorescence signals which are low relative to the detection limit of the photodetector system. Of the various types of image tubes, only image intensifiers provide significant light amplification. As gateable devices, image tubes are especially useful in pulsed PLIF measurements, where the luminous background, integrated over a millisecond (the duration of fast mechanical shutters) may be greater then the PLIF signal. With cw or quasi-cw lasers, the gating allows short integration times and precludes image smearing. As wavelength converters, image tubes convert the incident fluorescence, which is often in the blue and ultraviolet, to visible wavelengths, the spectrally sensitive range of many two-dimensional photodetectors. For most combustion applications, an S-20 photocathode and, for most solid-state detectors, a P-20 phosphor are suitable. The major disadvantage of image tubes, besides their cost and complexity, is their spatial resolution.

When image tubes or intensifiers are included in the detection system the phosphor image must be optically coupled to the array detector. It is possible to lens couple the image tube to the detector, but coherent fiber-optic bundles are usually preferred. The coupling magnification is easily changed in lens coupled systems, but lens coupling has three severe drawbacks in comparison to fiber-optic coupling: the numerical aperture, a measure of light gathering efficiency, of an $f/1$ lens, a lens with excellent collection efficiency, is only one-half, while fiber bundles can have numerical apertures near unity; focussing errors in low f-number lens systems severely reduce the spatial resolution; and rigid mounting and vibration reduction between the image tube and the photodetector is more difficult for lenses than for fiber bundles. Thus lens coupled systems tend to have poor collection efficiencies and poor spatial resolution compared to fiber-optically coupled detectors. A fiber-optic minifier, a tapered fiber bundle, is typically employed in order to match the spatial resolution of the image tube to the array. If fiber bundles are used to couple the intensifier and detector array, the array should be covered with a fiber-optic window. Unfortunately, this excludes the use of many, otherwise acceptable, detector arrays.

Most PLIF images are recorded with two-dimensional photodetector arrays, as opposed to photographic film. While film provides excellent spatial response and high data acquisition rates, it has a non-linear signal response and provides poor feedback (i.e. the capability for the user to quickly view and process acquired images). Also as mentioned above, the spatial resolution of the detection system is often

limited by the collection optics or the image intensifier. Under these circumstances, the high spatial response of film is no longer a significant advantage. Four basic types of array photodetectors are available for imaging applications. These are silicon intensified target (SIT) tubes, also known as vidicons, and three self-scanned solid-state devices: photodiode (PD), charged-coupled device (CCD), and charge-injected device (CID) arrays. CCD detection, and to a lesser extent PD detection, is most commonly used in current PLIF research. PD arrays exhibit less blooming than most of the other photodetectors, but usually have a higher readout noise. CCDs have superior noise and dynamic range performance, and are available in larger format arrays than PD detectors. A significant advantage of CCD systems is the increasing availability of low-cost CCD cameras operating under standard video formats and employing off-the-shelf hardware (e.g., frame-grabbers) and software.

3. Image Corrections

PLIF image data contain several systematic and random errors. The primary systematic errors which have received attention thus far are due to: (spatially) nonuniform sheet illumination, nonuniform pixel responsivity, nonuniform intensifier gain, and background and dark signal. For a detailed treatment of these and other error sources, see the papers by Paul et al. [33] and Hanson and Seitzman [35].

In summary, the sequence employed for correcting systematic errors in the recorded image is as follows. First, a combined image of the dark current and background signals is subtracted from the recorded image. Second, the new image is multiplied by a correction image accounting for spatial variations in the responsivity of the detector, which along with varying pixel offsets is called the fixed pattern noise. This correction includes combined variations in the array, intensifier, and amplifiers; and is typically measured by uniformly illuminating the detector system and comparing the signal at each pixel with the average signal. Third, non-uniformities in the laser sheet energy are included through another multiplicative factor. This factor may be determined on a shot-by-shot basis, for example with a calibrated linear array, if the sheet distribution varies significantly with time; or it may be measured in separate experiments with the PLIF detection system (once it is calibrated) if the sheet illumination is reproducible.

4. PLIF Strategies and Results

The flow-field parameters accessible with PLIF imaging include species concentration, temperature, velocity, pressure and density. Of course, once 2-D image data are available, other quantities can be computed from such field measurements. For example, gradients and dissipation factors may be obtained from species data; heat flux vectors are calculable from temperature data; and vorticity can be computed from 2-D velocity data. For each primary parameter, several PLIF strategies are possible, with the preferred approach often depending on local flowfield conditions, available equipment and the objectives of the study.

In many cases, only qualitative or flow structure information is sought from PLIF images, for example to reveal critical regions or interfaces in flows, such as flames, shock waves or recirculation zones. In other cases, the goal is to obtain quantitative information. Of course, image data are immediately quantitative with regard to position and time, and hence the use of PLIF for detailed study of flowfield structure, for example of turbulent jets or flames, is particularly promising. Such applications typically require computer-based image processing. Rendering PLIF data quantitative in terms of concentration, temperature or velocity is more difficult and constitutes one of the principal thrusts of current research.

In this section, we provide an overview of primary PLIF strategies, all based on single-photon excitation, and present sample results for imaging of species and temperature. Velocity, and combined velocity/pressure imaging has been demonstrated, but not yet in a combustion environment. Thus it is not discussed here; see the papers by Paul et al. [10] and Hiller and Hanson [11]. Density imaging is envisioned as a form of species imaging and hence is not discussed explicitly here. The extension of PLIF to multiphoton excitation is discussed in Sect. 5.

4.1. Species Imaging

The bulk of all PLIF imaging has been aimed at species measurements. In most cases thus far, the measurements have been qualitative rather than quantitative, in the sense that the data have not been converted to absolute species concentrations or number densities. This is due both to the difficulty of converting fluorescence signals to values for absolute concentration and to the fact that qualitative image data, like conventional flow visualization (e.g., schlieren or shadowgraph) data, have immediate value for building flowfield understanding. Thus qualitative species imaging, usually shown in the form of false color PLIF intensity maps, has proven an effective tool for locating flames, regions of burned or unburned gases, recirculation zones, shock waves, and so on.

The relationship (10) between the measured number of photons from a flowfield volume element and the

quantity of interest, namely the number density of the absorbing species, depends on: 1) temperature, which controls the Boltzmann fraction in the absorption step; 2) the fluorescence yield; and 3) several physical constants and fixed experimental parameters, such as optical collection efficiencies and detector response functions, which can be determined separately. The principal difficulty in rendering fluorescence quantitative is specifying the fluorescence yield, i.e. the fraction of absorbed photons which are re-emitted as fluorescence photons,

$$A_{21}/(A_{21}+Q_{21}).$$

Here Q_{21} denotes the sum of collisional quenching, predissociation and ionization loss rates, and may depend on the composition, temperature, and pressure of the gas mixture being probed.

There are many possible strategies for dealing with these issues; here we describe only the most common, beginning with the usual situation in which electronic quenching is the primary element in Q_{21} and the pressure of the mixture is high enough that Q_{21} dominates A_{21}. In this case, we represent Q_{21} by

$$Q_{21}=n\sigma\langle v\rangle,$$

where n is the total number density of the mixture, $\langle v\rangle$ is an appropriate mean molecular speed and σ is a mixture-averaged quenching cross-section. When the mixture and temperature are known within reasonable bounds, and cross-section data are available, absolute values for $\langle v\rangle$ and σ may be calculated and Q_{21} becomes a known function of n, and possibly temperature. In the more common case that the cross-sections are not available, particularly at elevated temperatures, we may simply choose to assume that σ is a constant (or has a specific temperature dependence). For example, if σ is taken as a constant, then Q_{21} is proportional to $nT^{1/2}$ and the fluorescence yield is proportional to $1/(nT^{1/2})$. Then the relationship between the fluorescence signal, in photons per pixel at the detector, reduces simply to [see (10)]

$$\begin{aligned}N_p&=\text{const}\cdot f_1(T)\chi_m n[1/(nT^{1/2})]\\&=\text{const}\cdot\chi_m[f_1(T)/T^{1/2}].\end{aligned}\tag{11}$$

In this limit, the fluorescence signal depends directly on the mole fraction of the species being probed and a known temperature-dependent function (in square brackets). The assumption of constant σ is useful, but must be carefully applied as electronic quenching can exhibit strong temperature and species dependence. In some situations, the appropriate quenching cross-section declines at elevated temperatures, with an approximate $T^{1/2}$ dependence, such that the bracketed term in (11) simplifies to $[f_1(T)]$.

These models of quenching lead directly to two common PLIF strategies. In the case that species imaging is the objective, a quantum state is selected which minimizes the overall temperature dependence of (11) in the temperature range of the experiment, and the measured signal is directly proportional to the species mole fraction. If only relative mole fraction is of interest, for example in studies of mixing, then the fluorescence intensity data can be used directly, after corrections for background signal and nonuniform sheet illumination. If absolute mole fractions are sought, a simple in situ calibration with a known mixture, for example using a flat flame burner or static sample, can be used to provide the missing proportionality factor. The second strategy apparent from (11) is to image a species with known mole fraction and intentionally choose a quantum state which produces a strong temperature dependence; then the fluorescence data can be used for temperature imaging (Sect. 4.2).

The other most common situation in rendering PLIF quantitative for species is to select excitation wavelengths which lead to predissociated upper states, for which the rate of predissociation dominates the collisional quenching. In this case, Q_{21} becomes a constant, independent of mixture composition, temperature and usually pressure, and the fluorescence yield is a constant. This measurement strategy is very attractive if one can afford the signal loss associated with a low fluorescence yield, but the reduced signal levels may prohibit this approach with trace species. Species amenable to this strategy include O_2 [22, 36], NO, H_2O, and OH [37]. Finally, we note that a very similar strategy could be employed with controlled photoionization from the upper level; this particular approach is known as PICLS when applied to single-point fluorescence measurements [23].

Several different species have been imaged using PLIF in combustion systems, generally using the simple temperature-independent strategy outlined above. With this approach the fluorescence intensities are directly proportional to species mole fraction. In isobaric flows, the data may be viewed as either mole fraction or partial pressure, and of course through selection of a transition with an additional T^{-1} temperature dependence [i.e. $f_1(T)\propto T^{-1/2}$], the PLIF signal can be made directly proportional to species number density (concentration). For nonreacting flows, this measurement strategy yields images of mass density.

Examples of PLIF species imaging of OH in atmospheric pressure H_2-air diffusion flames are shown in Fig. 3 [38]. These images were obtained using single 10 ns, 50–100 mJ pulses from a narrow-linewidth XeCl excimer laser tuned to excite the $Q_1(3)$ line of OH at $\lambda=308.2$ nm in the (0,0) band of the $A\leftarrow X$ system.

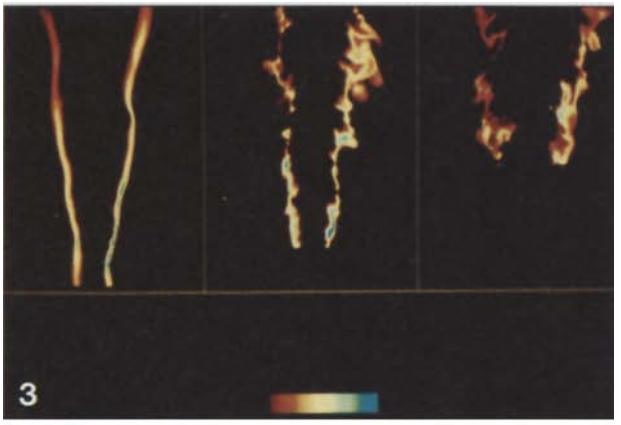

Fig. 3. PLIF images of OH in a turbulent hydrogen/air nonpremixed flame. From left to right, jet exit Reynolds numbers, Re_D, are 2300, 25000, and 50000. The images are displayed in false color, with the color map shown in the lower horizontal bar, blue is high signal and black is no signal. From [38]

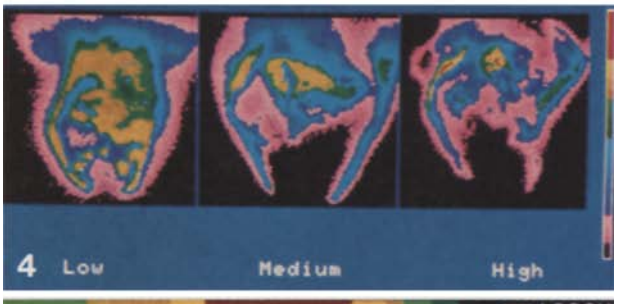

Fig. 4. Instantaneous (10 ns) images of the OH distribution in the central plane of a *n*-heptane/air spray flame, with the atomizing air flow rate increasing from the left to right image. The region viewed is 8×8 cm, and the false color map is indicated at the right. From [6]

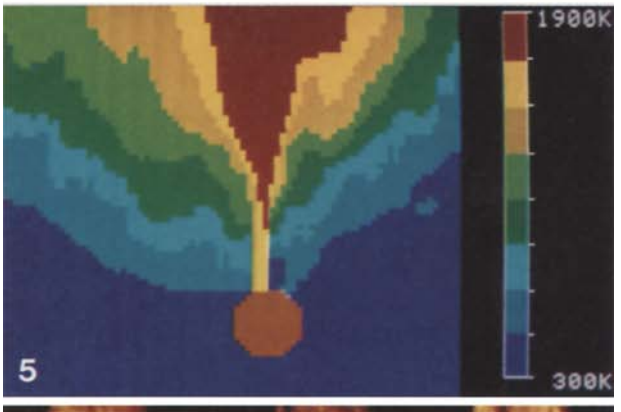

Fig. 5. Temperature contours for a 9.6×9.6 mm region in a rod-stabilized (1.5 mm diameter) methane-air flame, measured using PLIF of NO. Scattering from the rod, indicated at the bottom of the image, corrupts the temperature measurements just upstream. A falso color display divides the flame into 200 K contours, from 300 K to 1900 K. From [7]

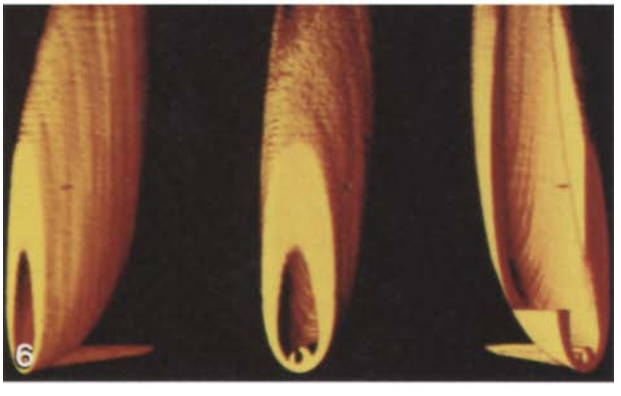

Fig. 6. Three-dimensional rendering of a diffusion flame resulting from a horizontal hydrogen jet in a crossflow of air and measured using PLIF of OH. The cylindrical object at the bottom of each view is an artifact produced by laser-scattering from the hydrogen fuel tube. The effect of a non-responsive pixel is also evident halfway up the flame

The laser sheet is oriented vertically on the centerline above the 2 mm inner diameter fuel tube, and the size of the region imaged is 5.8 cm × 7.7 cm × 0.3 mm (laser sheet thickness). The laser linewidth ($\sim$0.5–1.0 cm^{-1} FWHM) is broad enough to fully encompass the absorption line so that the absorption lineshape parameters need not be known. The three cases illustrated were obtained with cold jet Reynolds numbers of (from left to right) 2300, 25000, and 50000, with the latter flame formed from a supersonic, $M = 1.3$,

hydrogen jet. The images show clearly the influence of increased turbulence levels and lift-off height at high Reynolds number.

The collection optics utilized a 105 mm focal length, $F/5.6$ aberration-corrected UV camera lens. The camera was an intensified, single MCP, CCD array, with 240×610 pixels in the imaging region. This frame-transfer CCD operates at a framing rate of 60 frames per second. The camera pixels are 10 μm wide $\times$ 18.5 μm in height, so that the overall dimensions of the array are 6×4.5 mm. In this case, a 2:1 tapered fiber-optic bundle was used between the 18 mm diameter intensifier and the array (diagonal dimension of 7.5 mm). The computer was an PC/AT compatible equipped with a frame grabber which digitizes the output to 8 bits in a format of 240×512 pixels.

In terms of characterizing the performance of the PLIF system, the important observations to be drawn from the images in Fig. 3 are that the SNR is excellent, in excess of 30 for the largest signals, and that the spatial resolution is sufficient to clearly define the instantaneous structure of these flames. The peak number of photons per pixel at the photocathode of the intensifier is about 10^4 and the signals are shot noise limited. Although the peak OH mole fraction in these flames is only known approximately (10,000 ppm), the PLIF images, shown here in false color, could be put on an absolute scale using a flat flame burner for calibration. Much of the interest in such flames is concerned with the appearance of flowfield structures (e.g., shape, thickness, and curvature), however, and in this regard the data are already quantitative.

A second example of species imaging, illustrating the use of nonresonant detection to exclude elastically scattered light, Fig. 4 presents the first imaging results obtained in a spray flame [6]. These measurements, of OH, were obtained relatively early in the development of PLIF and used a Nd:YAG-pumped dye laser source (10 mJ, 0.5 cm^{-1} linewidth) and an intensified 100×100 photodiode array camera. The single-shot images were obtained for an 8×8 cm region on the central axis of an atmospheric pressure, air-atomized *n*-heptane spray flame. The OH was excited via the $Q_1(5)$ transition in the (1,0) band at 283 nm; broadband fluorescence from the (1,1) band near 316 nm was detected through a 10 nm bandpass filter (with a transmission of 10^{-4} at the laser wavelength). This scheme provided relatively high values of SNR as well as effective isolation from the strong elastic scattering of laser light by the droplets present in the illumination zone.

The demonstration of OH imaging in a spray flame was an important milestone in the development of PLIF, owing to the importance of liquid fuel combustion and to the failure of other laser-based diagnostic techniques in such environments. Additionally, the results obtained provide a clear demonstration of the utility of PLIF for characterizing complex, unsteady combustion processes. For example, the images in Fig. 4 reveals at least three primary regions of the flow: a relatively cold region above the nozzle in which the fuel is evaporating without combustion; a relatively thin sheath of flame located at the periphery of the spray where entrainment of surrounding air provides sufficient oxidizer to support combustion; and a relatively large but spatially and temporally nonuniform central region of combustion. By allowing partial transmission of elastically scattered light, it was possible to show that residual droplets were present in this region and that combustion occurred primarily in semi-isolated packets of fuel and air. In addition, images of both CH (using excitation at 431 nm) and C_2H_2 (multiphoton photodissociation at 193 nm) were obtained in this study [6]; the former (CH) serves as a more direct indication of the instantaneous flame zone than OH, while the acetylene serves to mark regions of fuel pyrolysis just upstream of a flame. Although the OH imaging system was not calibrated to yield absolute concentration, the peak OH levels were established to be about 1000 ppm. Even without calibration, however, PLIF imaging is clearly capable of providing critical and unique insight into fundamental spray combustion processes.

4.2. *Temperature Imaging*

Since most combustion flows are unsteady, the objective of a temperature diagnostic should be to obtain instantaneous images. There are at present two basic strategies [39] for such measurements: (1) two-line methods, which utilize two excitation wavelengths (i.e., two lasers) to infer temperature; and (2) monochromatic (i.e., single-laser) excitation methods. Only the latter has actually been demonstrated in a form providing instantaneous 2-D measurements.

In the simplest variation of the two-line strategy, a pair of excitation wavelengths is used to produce separate broadband fluorescence signals arising from two distinct lower states of the same species. The ratio of the fluorescence intensities is proportional to the relative populations in the absorbing states [see (11)] and hence is a function of temperature through Boltzmann statistics, assuming that the distribution function for the energy mode in question is in equilibrium. Ideally, the two transitions utilized have the same upper state so that possible differences in fluorescence yields are nullified. The primary difficulty with this approach, and the principal reason why the method has not yet been demonstrated, is simply that two laser sources and, generally, two camera systems

are required if the measurement is to be effectively instantaneous. The cost of tunable pulsed laser systems and intensified solid-state cameras and the overall complexity of such a set-up is somewhat prohibitive. The concept for temperature imaging has been demonstrated, however, in flames using PLIF ratios of OH acquired at different times with a single tunable laser source. Since the flat flame burner utilized was nominally steady, it was possible to adjust the dye laser to a new wavelength and acquire a second PLIF image without substantial change in flow conditions [40].

There are two primary variations of the monochromatic-excitation strategy. The first variation, not yet demonstrated in an imaging experiment, is to excite (an atomic or molecular species) with one laser source but to detect fluorescence in two separate spectral channels. The ratio of such signals can be a sensitive indicator of temperature, but requires rapid collisional transfer from the upper level to achieve a broad distribution over adjacent states. The obvious difficulty with such a scheme is that it may depend on unknown collisional relaxation rates and hence could require careful calibration, but single-point LIF thermometry of atomic seeds in flames has yielded impressive results (see the review paper by Laurendeau [39]).

A second monochromatic method outlined above, relying primarily on the temperature dependence of the population fraction in the absorbing state, has also been investigated. Two successful PLIF measurements of this type have been reported; both required only one laser and one camera, but also were limited to flows with a fixed mole fraction of the absorbing species. In one case, temperature was imaged with a single laser shot in a turbulent rod-stabilized flame by exciting NO which had been seeded into the premixed CH_4-air mixture at a fixed level. As long as the mole fraction remains relatively fixed, as occurs for example under fuel-lean conditions, the PLIF signal becomes a known function of temperature [see (11)]. An example result is shown in Fig. 5 [7]. Here the $Q_1(22)$ $A \leftarrow X$ transition of NO was pumped with 2 mJ of laser energy at 225.6 nm. This particular transition provided reasonable sensitivity to temperature in the range of interest and was additionally attractive since it enabled a self-calibration strategy. As the function $f_1(T)/T^{1/2}$ has a maximum at a temperature of 740 K, peak signals in the image can immediately be identified with this temperature, and lower signals can be converted to absolute temperature through their ratio with the peak signal and the known temperature dependence of this function. Although there are potential difficulties with the double-valued nature of the signal on temperature, this was not a problem in the flow studied. The primary limitation of the method is that of identifying a suitable inert tracer with an acceptable excitation/fluorescence spectrum.

The other demonstration of monochromatic temperature imaging was based on multiple-line excitation of vibrationally excited O_2 in the $B \leftarrow X$ Schumann-Runge system [8]. A broadband (0.8 nm) argon fluoride excimer laser (193 nm) was used as the excitation source, and the resulting broadband fluorescence was collected using an intensified 100×100 pixel camera. A number of oxygen transitions are excited at this wavelength, involving excited vibrational states. The result is a strong, monotonic dependence of the fluorescence signal on temperature, as described by Lee and Hanson [36]. As with the NO study cited above, the primary limitation of this scheme is its requirement for a fixed mole fraction of the species monitored, or a simultaneous PLIF measurement of the mole fraction.

5. Multiphoton Excitation

Many species important in combustion have transitions which are spectrally inaccessible with single-photon excitation LIF. Most significant atoms and a number of diatomic molecules have single-photon resonance transitions in the deep ultraviolet (UV) and vacuum UV regions. Producing laser radiation at these wavelengths and then transmitting it through atmospheric and combustion gases is exceedingly difficult. As an alternative, techniques based on multiphoton excitation, followed by single-photon fluorescence detection have recently been adopted.

Although the excitation process is generally much weaker than with allowed single-photon processes, satisfactory LIF and PLIF signals can be generated using intense laser sources or multipass optical arrangements. The intense laser pulses required can cause photochemical perturbations, however, and this effect along with possible photoionization processes should be included in a proper LIF model [24]. Besides access to deep and vacuum UV transition, multiphoton excitation embodies other advantages. Generally, the detected fluorescence is sufficiently shifted to longer wavelengths such that typical interferences, for example elastically scattered laser light, are avoided. Additionally, controlled photoionization of the upper state can serve as a means of avoiding uncertainties in collisional quenching, as discussed in sect. 4.1.

Two-photon laser-induced fluorescence has been used for single-point flame detection of oxygen [28, 41] and hydrogen [42] atoms, and OH [43, 44] molecules. In addition, one-dimensional imaging of O and H atoms [45, 46] and CO [47] have been demonstrated.

The only example of multiphoton PLIF, to our knowledge, is the study by Seitzman et al. [24] in a CO-air laminar diffusion flame. Two-photon excitation of CO at 230.1 nm from the $X^1\Sigma^+$ to the $B^1\Sigma^+$ state produced fluorescence to various vibrational levels of the $A^1\Pi$ state, at wavelengths from 451 to 725 nm. Good quality, single-shot images were obtained with a laser energy of only 2 mJ per pulse at the entrance to a multipass cell, which served both to maintain the beam intensity over a large region and to provide a more uniform intensity distribution than obtained in a single-pass configuration. In this experiment, the CO fluorescence was a function of both CO mole fraction and temperature. Theoretical predictions of the temperature dependence and thermocouple measurements of the temperature profile were used to convert the fluorescence data to CO mole fraction. The agreement between the PLIF results and CO mole fractions measured by infrared analysis of sampled gases was good, with a maximum relative discrepancy of 20%.

6. Image Processing

In addition to the useful flow visualization aspects of PLIF, a wealth of quantitative information is contained in each image. Since the images are acquired as digital representations and stored on computers, the most efficient and powerful method for extracting this information is computerized image processing. Image correction is typically the first stage of processing. After a PLIF image is corrected and converted to a field measurement, to mole fraction for example, further image processing can yield additional information.

Conventional image processing techniques are typically directed toward image enhancement, image transmission and pattern recognition [48]. Though some of these standard methods are applicable to PLIF images, combustion scientists and engineers are more typically interested in extracting information like scalar dissipation, flame strain, and flame thickness. Algorithms for interrogating PLIF images are evolving in parallel with the new generated by the availability of instantaneous, spatial field measurements [49].

Image processing for flowfield analysis is demonstrated in the study of turbulent mixing by van Cruyningen et al. [50]. Here, biacetyl was added to an atmospheric-pressure N_2 jet (5% biacetyl) issuing from a 1 cm diameter nozzle, with $Re = 8500$. Images of the jet fluid mixing with a coflowing stream of N_2 in a 60×60 cm tunnel were obtained with a high-resolution (384×576 by 14-bits) CCD array camera. The minimum and maximum detectable signals were 140 and 50000 ppm, respectively, providing a dynamic range of 3500. Various processing techniques were applied to the high quality images obtained in this study, including the algorithm outlined in Sect. 3 to correct for nonuniformities and background. A distance-dependent multiplicative scaling was applied to account for the self-similar ($1/x$) downstream development of the jet. Radial concentration profiles at different axial locations were derived for both instantaneous and time-averaged images, revealing a uniformly mixed jet (for each axial location) which appears on a time-averaged basis to have a gaussian concentration profile because of side-to-side motion, i.e. flapping. Images of scalar dissipation were produced by computing spatial derivatives, and the maximum average scalar dissipation was found to occur along lines at an angle of 45° to the jet axis. Again, the high spatial and signal resolution in the acquired images contributed greatly to the success of these image processing techniques.

Another application of image processing is the extraction of structural information from images. Since an image is a spatial record, imaging is an ideal technique for investigating the behavior of spatial objects, for example the interaction of turbulent eddies and flame fronts. For example, Fourier transform methods have been applied to determine spatial correlations [38]. The goal of that study was to investigate organized spatial structures in a turbulent ($Re_D \approx 2300$–50000) non-premixed hydrogen jet burning in air. In this flame, the OH radical is found at super-equilibrium concentrations near the flame front and is also found at lower concentrations in hot product gases. Thus, the OH molecule is a good marker of the flame zone and is also expected to mark the high vorticity regions of the flame jet. Characteristic scale sizes and flame angles were measured from two-dimensional spatial autocorrelation images. The autocorrelations were computed using fast Fourier transform algorithms. Reynolds number invariance in the axial length scale (parallel to the flame zone) was observed. The axial scale size initially decreased with increasing Reynolds number, then became constant at a Reynolds number greater than approximately 2×10^4.

The use of image processing in connection with 3-D measurements is illustrated in Fig. 6. A horizontal jet of hydrogen was directed into a higher velocity, vertical stream of air. A 3-D data set ($94 \times 71 \times 32$ mm) of the diffusion flame resulting from these jets in crossflow was compiled by sequentially recording 32 individual vertically-oriented planes of OH data equally spaced along the horizontal axis of the hydrogen jet. Each plane of OH data (240×512 pixels) was recorded with an image-intensified CCD array camera and averaged

over 25 laser pulses. The 32 images were then interpolated to form a volume consisting of 160 planes. Figure 6 applies surface rendering of the resulting OH volume to display the 3-D data set, with the surface displayed at three separate orientations. In this display, a virtual light source was added above and to the left of the image to provide shading. This is one of the cues provided for depth perception in rendered displays. Rotation of the image adds to the depth perception and enhances interpretation of the data. A cut-away in the rightmost view allows simultaneous observation of the inner surface. These techniques can be utilized along with interactive, real-time computer displays for investigation of more complex structures.

7. Conclusions – Trends in Planar Imaging

Imaging diagnostics have already had a significant impact on combustion research, and their use is likely to increase in the future. Planar fluorescence imaging, in particular, is likely to grow in significance owing to its species specificity, relatively high sensitivity, and versatility for monitoring several flowfield parameters using the same equipment. Although progress may be expected on several fronts, measurement objectives of particular note include extensions of PLIF: to monitor new variables (such as pressure and density), to function in new environments (such as hypersonic flows), and to measure multiple parameters simultaneously (such as velocity, temperature, density and species composition).

Finally, we note that the continuing developments in laser sources, solid-state cameras and laboratory computers are likely to significantly impact PLIF capabilities and research activities. With regard to lasers, improved access to UV wavelengths is especially important, since many critical combustion species must be excited in this spectral region. Two outstanding recent developments in this direction include: frequency-doubling crystals with increased efficiency at short wavelengths, and tunable, high-pulse-energy excimer lasers. The use of Raman-shifted excimer lasers is likely to be especially important in single-photon-excitation imaging of species such as O_2, NO, OH, and in multiphoton excitation of species such as H_2O, CO, O, H, and N_2. In addition to these developments, advances in other lasers, particularly solid-state lasers, are likely to lead to more compact and economical tunable laser sources, and those improvements will surely lead to increased usage of PLIF imaging such as combustion monitoring applications.

The area of camera technology is central to PLIF imaging, and impressive advances are being made in the performance, convenience, cost and system packaging of solid-state detector array systems. In particular, we cite the trend toward high-resolution, low-noise CCD arrays, with cameras having 1/2 to 1 megapixels now seeing initial use in laboratory PLIF experiments and cameras with 16 megapixels having been recently announced. New cameras also feature more convenient architecture, particularly with regard to interfacing with laboratory computers. The use of video-format CCD cameras and frame grabbers greatly alleviates the difficulties of set-up and operation of the camera system. A critical problem at present in the limited availability of solid-state cameras fitted with fiberoptic stubs for direct coupling to MCP intensifiers, but the trend toward increased commercial availability of such cameras is positive.

The trend toward increasingly powerful, economical laboratory computers will lead to important improvements in data acquisition and processing speeds as well as image data storage capability. The result will be routine use of PLIF for acquiring large data sets which can be processed to determine statistical properties of image data, rather than the current situation in which only a few images are typically acquired and processed. These improvements will also encourage the use of PLIF in applications-oriented work.

Acknowledgements. The authors are pleased to acknowledge the important contributions made to Stanford's imaging diagnostics program by several graduate students and colleagues, particularly G. Kychakoff, R. Howe, M. Allen, B. Hiller, M. Lee, D. Hofeldt, B. McMillin, and J. McDaniel. Our research has been sponsored by the U.S. Air Force Office of Scientific Research, Aerospace Sciences Directorate.

References

1. M.B. Long, B.F. Webber, R.K. Chang: Appl. Phys. Lett. **34**, 22–24 (1979)
2. M. Aldén, H. Edner, G. Holmsted, S. Svanberg, T. Hogberg: Appl. Opt. **21**, 1236–1240 (1982)
3. M.J. Dyer, D.R. Crosley: Opt. Lett. **7**, 382–384 (1982)
4. G. Kychakoff, R.D. Howe, R.K. Hanson, J.C. McDaniel: Appl. Opt. **21**, 3225–3227 (1982)
5. L.A. Melton, J.F. Verdieck: Combust. Sci. Technol. **42**, 217–222 (1985)
6. M.G. Allen, R.K. Hanson: In *Twenty-first Symposium (International) on Combustion* (The Combustion Institute 1986) pp. 1755–1761
7. J.M. Seitzman, G. Kychakoff, R.K. Hanson: Opt. Lett. **10**, 439–441 (1985)
8. M.P. Lee, P.H. Paul, R.K. Hanson: Opt. Lett. **12**, 75–77 (1987)
9. J.C. McDaniel, B. Hiller, R.K. Hanson: Opt. Lett. **8**, 51–53 (1983)
10. P.H. Paul, M.P. Lee, R.K. Hanson: Opt. Lett. **14**, 417–419 (1989)

11. B. Hiller, R.K. Hanson: Appl. Opt. **27**, 33–48 (1988)
12. R.K. Hanson: In *Twenty-first Symposium (International) on Combustion* (The Combustion Institute 1986) pp. 1677–1691
13. A. Yariv: Quantum Electronics (Wiley, New York 1975)
14. W. Demtröder: Laser Spectroscopy (Springer, Berlin, Heidelberg 1982)
15. R.P. Lucht: In *Laser Spectroscopy and its Applications*, ed. by L.J. Radziemski, R.W. Solarz, J.A. Paisner (Dekker, New York 1987) pp. 623–676
16. A.C. Eckbreth: Laser Diagnostics for Combustion Temperature and Species (Abacus, Kent 1988)
17. E.H. Piepmeier: Spectrochim. Acta **27B**, 431–443 (1972)
18. J.W. Daily: Appl. Opt. **16**, 2322–2327 (1977)
19. R. Altkorn, R.N. Zare: Annu. Rev. Phys. Chem. **35**, 265–289 (1984)
20. E.H. Piepmeier: Spectrochim. Acta **27B**, 445–452 (1972)
21. H. Greenstein, C.W. Bates, Jr.: J. Opt. Soc. Am. **65**, 33–40 (1975)
22. M.P. Lee, P.H. Paul, R.K. Hanson: Opt. Lett. **11**, 7–9 (1986)
23. J.T. Salmon, N.M. Laurendeau: Appl. Opt. **26**, 2881–2891 (1987)
24. J.M. Seitzman, J. Haumann, R.K. Hanson: Appl. Opt. **26**, 2892–2899 (1987)
25. R.J. Cattolica: Appl. Opt. **20**, 1156–1166 (1981)
26. R.P. Lucht, D.W. Sweeney, N.M. Laurendeau: Appl. Opt. **19**, 3295–3300 (1980)
27. P.M. Doherty, D.R. Crosley: Appl. Opt. **23**, 713–721 (1984)
28. A.W. Miziolek, M.A. DeWilde: Opt. Lett. **9**, 390–392 (1984)
29. J.E.M. Goldsmith: Appl. Opt. **28**, 1206–1213 (1989)
30. G. Meijer, J.J. ter Meulen, P. Andresen, A. Bath: J. Chem. Phys. **85**, 6914–6922 (1986)
31. L.R. Boedeker: Opt. Lett. **14**, 473–475 (1989)
32. J. Haumann, J.M. Seitzman, R.K. Hanson: Opt. Lett. **11**, 776–778 (1986)
33. P.H. Paul, I. van Cruyningen, R.K. Hanson, G. Kychakoff: Exp. Fluids (in press)
34. J.L. Wiza: Nucl. Instrum. Methods **162**, 587–601 (1979)
35. R.K. Hanson, J.M. Seitzman: In *Experiments in Combustion*, ed. by A. Taylor (Academic, London, in press)
36. M.P. Lee, R.K. Hanson: J. Quant. Radiat. Transfer **36**, 425–440 (1986)
37. P. Andresen, A. Bat, W. Gröger, H.W. Lülf, G. Meijer, J.J. ter Meulen: Appl. Opt. **27**, 365–378 (1988)
38. J.M. Seitzman, A. Üngüt, P.H. Paul, R.K. Hanson: AIAA-90-0160, AIAA Aerospace Sciences Meeting, Reno (1990)
39. N.M. Laurendeau: Prog. Energy Combust. Sci. **14**, 147–170 (1988)
40. R.J. Cattolica, D.A. Stephenson: Prog. Astro. Aero. **95**, 714–721 (1985)
41. M. Aldén, H. Edner, P. Grafstrom, S. Svanberg: Opt. Commun. **42**, 244–246 (1982)
42. R.P. Lucht, J.T. Salmon, G.B. King, D.W. Sweeney, N.M. Laurendeau: Opt. Lett. **8**, 365–367 (1983)
43. D.R. Crosley, G.P. Smith: J. Chem. Phys. **79**, 4764–4773 (1983)
44. J.E.M. Goldsmith, N.M. Laurendeau: Appl. Opt. **25**, 276–283 (1986)
45. M. Aldén, H.M. Hertz, S. Svanberg, S. Wallin: Appl. Opt. **23**, 3255–3257 (1984)
46. J.E.M. Goldsmith, R.J.M. Anderson: Appl. Opt. **24**, 607–609 (1985)
47. M. Aldén, S. Wallin, W. Wendt: Appl. Phys. B **33**, 205–208 (1984)
48. W.K. Pratt: Digital Image Processing (Wiley, New York 1978)
49. R.N. Strickland, D.W. Sweeney: Appl. Opt. **27**, 5213–5220 (1988)
50. I. van Cruyningen, A. Lozano, R.K. Hanson: ASME Winter Annual. Meeting, San Francisco (1989)